Simulation of a Crossover from the Precipitation Wave to Moving Liesegang Pattern Formation

Ferenc Izsák[†,‡,§] and István Lagzi*[,||]

Department of Applied Analysis, Eötvös University, P.O. Box 120, Budapest H-1518, Hungary, Department of Applied Mathematics, University of Twente, The Netherlands, and Department of Physical Chemistry, Eötvös University, P.O. Box 32, Budapest H-1518, Hungary

Received: July 1, 2004; In Final Form: October 29, 2004

Model simulations to investigate the precipitation wave phenomenon and a crossover from the precipitation wave to moving Liesegang patterns were performed. The chemical scheme contains four chemical species via the interaction of precipitation and redissolution (complex formation), in which the precipitation reaction term was based on Ostwald's supersaturation theory. In this article, for the first time, all the features and behaviors of the heterogeneous traveling waves are reproduced, which were observed experimentally in the work of Zrínyi et al. (Zrínyi, et al. *J. Phys. Chem.* **1991**, *95*, 1618.). The detailed investigation of the pattern formation showed three possible states of the system, which depend on the initial concentration of the inner and outer electrolytes, respectively. These are the precipitation wave (single moving precipitation band), the moving Liesegang pattern (moving precipitation bands), and the state where these two patterns coexist.

1. Introduction

The coupling of diffusion with chemical reactions often results in chemical pattern formation. One of these reaction−diffusion systems is the Liesegang pattern formation.[1] These patterns are produced by a precipitation reaction behind a diffusion front. The Liesegang pattern formation mechanism was proposed to explain similar phenomena in geoscience (structure of agate rocks)[2] and in medicine (gallstones).[3] An electrolyte, called an outer electrolyte, diffuses into a reaction medium (in the experiments, it is usually a gel) and reacts with another electrolyte (inner electrolyte) that is uniformly distributed in the reaction medium. The precipitation reaction between them produces an insoluble and immobile precipitate product, which is distributed quasi-periodically in the reaction medium.

The models describing Liesegang pattern formation can be divided into two categories. They are either microscopic (usually stochastic)[4−7] or macroscopic. Microscopic (or discrete) models treat the reacting particles individually both in the reactions and in the diffusion process via the utilization of Brownian motion. Brownian motion (or random walk) of particles is a usual mathematical model of diffusion in microscopic models. These sophisticated models incorporate the inherent fluctuations of the system and provide a detailed description of the precipitation process.[4−7] These models are realistic only if a great number of particles is taken, and this requirement leads to a high computational cost. Macroscopic models of Liesegang pattern formation focus on the solution of mean-field equations (usually reaction−diffusion equations) by the appropriate numerical methods.[8−15] In the literature, one can find some deterministic mathematical descriptions, in which fluctuations are incorporated.[16,17] Recently, using such an approach, the behavior of the stochastic precipitation pattern formation at low initial concentration differences of the outer and inner electrolytes was reproduced.[17]

The chemical mechanisms for describing the precipitate formation may contain consecutive steps. In the simplest case, the outer electrolyte (A) and the inner electrolyte (B) form directly the precipitate (AB), without any intermediate steps ($A + B \rightarrow AB$). The intermediate species mechanism incorporates an intermediate species (C) and an intermediate reaction step ($A + B \rightarrow C \rightarrow AB$).[18,19] C is assumed to be a colloid particle (sol), which is produced from the electrolytes continuously, and then, AB forms from C.

Different types of models are proposed to explain the Liesegang pattern formation.[20] The first developed and the simplest approach is the "prenucleation" theory (*Ostwald's model* based on Ostwald's idea[21−24]). In this model, the nucleation and precipitation processes are not separated in space and time. Nucleation is a spatially discontinuous phenomenon; nucleation is assumed to occur only at prospective band positions. The nucleated particles grow and deplete the electrolyte concentrations in their surroundings. More complex is the "postnucleation" theory, in which the bands evolve through precipitate growth and ripening after the terminated nucleation phase (e.g., *competitive particle growth* (CPG) model).[25−27]

Another theoretical approach to simulate the precipitate formation is the phase separation based on the Cahn−Hilliard equation.[16,28]

In the classical experiments, Liesegang patterns are "static"; this means that the position of the bands does not change during the evolution of the diffusion front. In the past decade, more complex pattern formation phenomena (compared to the regular Liesegang structures) were observed and investigated. In some cases, precipitation bands can redissolve in excess invading electrolyte due to the complex formation. Both effects cause the motion of the individual band or the band system along the diffusion column.[29] One can observe a *moving Liesegang pattern* when several bands advance due to the dissolution of bands (by the complex formation of precipitate) behind the pattern and new ones form (by precipitation) in front of the pattern. Sometimes, we can detect only a single evolved band (pulse) instead of a band system; this phenomenon is called (heterogeneous) precipitation wave.[30] The appearance of these different types of patterns depends on the compounds of the chemical

* Corresponding author. E-mail: lagzi@vuk.chem.elte.hu.
† Department of Applied Analysis, Eötvös University.
‡ University of Twente.
§ E-mail: izsakf@cs.elte.hu.
|| Department of Physical Chemistry, Eötvös University.

10.1021/jp047111v CCC: $30.25
Published on Web 01/15/2005

system and on the initial concentrations of the electrolytes. From the chemical point of view, the mechanisms, which produce such patterns, can be grouped into two types.

(i) In the systems $NaOH/Cr(NO_3)_3$[30−32] or $KI/HgCl_2$[33] (outer/inner electrolytes), the formed precipitate ($Cr(OH)_3$(s) or HgI_2(s)) reacts with the outer electrolyte (OH^-/I^-) and produces $[Cr(OH)_4]^-$(aq) or $[HgI_4]^{2-}$(aq) by redissolution in excess OH^- or I^-.

(ii) In the $NH_4OH/CoCl_2$ system, the reaction between Co^{2+}(aq) and OH^-(aq) forms $Co(OH)_2$(s), which reacts with ammonia, yielding $[Co(NH_3)_6]^{2+}$(aq). Here, the complex forming species (ammonia) is not the precipitate forming species (OH^-).[34−37]

Experimentally, in system i, mostly precipitation waves were observed, and in system ii, moving Liesegang pattern (bands) were observed. Zrínyi et al.[30] reported that the thickness of the precipitation wave in the experiments was constant within the experimental error during the development of the moving band. They found that increasing the concentration of the inner electrolyte resulted in slower motion. Furthermore, the authors observed the development of Liesegang patterns in the case of low electrolyte concentrations.

The aim of the present work is to reproduce all features of the precipitation wave phenomenon, which was observed experimentally,[30] and to show for the first time the direct crossover from the precipitation wave to moving Liesegang patterns.

2. Model

For describing moving pattern formation, many chemical mechanisms have been proposed; a simple and generic one is the following:

The diffusive reagents A(aq) (outer electrolyte) and B(aq) (inner electrolyte) turn into the immobile precipitate AB(s) by

$$\mathrm{A(aq)} + \mathrm{B(aq)} \rightarrow \mathrm{AB(s)} \tag{1}$$

The precipitate AB(s) can redissolve in the excess of the outer electrolyte due to the complex formation by

$$\mathrm{AB(s)} + \mathrm{A(aq)} \rightarrow \mathrm{A_2B(aq)} \tag{2}$$

where A_2B(aq) is the complex. The experiments are carried out in a gel matrix: the role of the gel is to prevent the sedimentation of the precipitate and convection. Zrínyi et al.[30] reported that the complex (here, A_2B(aq)) is trapped by the gel chains. Therefore, the precipitate and the complex cannot diffuse in the diffusion column. However, it should be noted that the immobilization of the complex is not a necessary condition for the moving pattern formation. Evolution of the above system in 1D can be described by the following reaction−diffusion equations; all quantities are dimensionless:

$$\frac{\partial c_A}{\partial \tau} = D_A \frac{\partial^2 c_A}{\partial x^2} - \Delta(c_A c_B, K, L) - k c_{AB} c_A \tag{3a}$$

$$\frac{\partial c_B}{\partial \tau} = D_B \frac{\partial^2 c_B}{\partial x^2} - \Delta(c_A c_B, K, L) \tag{3b}$$

$$\frac{\partial c_{AB}}{\partial \tau} = \Delta(c_A c_B, K, L) - k c_{AB} c_A \tag{3c}$$

$$\frac{\partial c_{A_2B}}{\partial \tau} = k c_{AB} c_A \tag{3d}$$

where c_A, c_B, and c_{A_2B} are the concentrations of the outer electrolyte, the inner electrolyte, and the complex, respectively, and c_{AB} is the amount of the precipitate depending on time (τ) and the space variable (x). k is the reaction rate constant for the complex formation (eq 2). D_A and D_B denote the diffusion coefficients of the electrolytes. To describe the precipitation formation presented by eq 1, we chose the model proposed by Büki et al.[12,13] based on Ostwald's ion-product supersaturation theory.[21] $\Delta(c_A c_B, K, L)$ is the precipitation reaction term defined as follows:

$$\Delta(c_A c_B, K, L) = \begin{cases} \kappa S_{AB} \Theta(c_A c_B - K) & \text{if } c_{AB} = 0 \\ \kappa S_{AB} \Theta(c_A c_B - L) & \text{if } c_{AB} > 0 \end{cases} \tag{4}$$

where κ is the rate constant of the precipitation reaction, K is the nucleation product, L is the solubility product, and Θ is the Heaviside step function. S_{AB} is the amount of the precipitate which can form, defined by the following algebraic equation:[12,13]

$$S_{AB} = \frac{1}{2}[(c_A + c_B) - \sqrt{(c_A + c_B)^2 - 4(c_A c_B - L)}] \tag{5}$$

Equation 5 can be derived assuming that the product of the reduced local concentrations of the electrolytes must be equal to the solubility product, that is, $(c_A - S_{AB})(c_B - S_{AB}) = L$. Using the relations $c_A, c_B > S_{AB}$, we obtain eq 5. The amount of the precipitate is determined by the difference $c_A c_B - L$ appearing in eq 5. If $c_{AB} = 0$, then a higher threshold (K) (nucleation product) should be applied in eq 4, but in any case, the procedure is driven by the (lower) solubility product (L).[12,13] The basis of the model is that precipitation occurs only if the product of the concentrations reaches K. However, if previously formed precipitate is present, it promotes the precipitation process; therefore, in this case, the product of the concentrations has to reach only a lower threshold (L) for precipitation. Precipitate formation was limited in the simulations ($c_{AB_{max}}$); if $c_{AB} > c_{AB_{max}}$, the precipitation process was stopped. Equation 3 has been solved numerically using a "method of lines" technique. We can reduce the set of partial differential equations (eq 3) to a set of ordinary differential equations after spatial discretization on an equidistant 1D spatial grid. The produced ordinary differential equations have been integrated in time using the second-order Runge−Kutta method with the following boundary conditions:

$$c_A|_{x=0} = c_{A0}, \quad \left.\frac{\partial c_B}{\partial x}\right|_{x=0} = \left.\frac{\partial c_A}{\partial x}\right|_{x=l} = \left.\frac{\partial c_B}{\partial x}\right|_{x=l} = 0$$

where l is the length of the diffusion column. In all simulations, we used the parameter set $D_A = D_B = 1.0$, $K = 0.103$, $L = 0.1$, $k = 10^{-3}$, $\kappa = 1.0$, $c_{AB_{max}} = 5.0$, and $l = 2200$. The initial conditions were

$$c_A(0, x) = c_{A0}\Theta(-x), \quad c_B(0, x) = c_{B0}\Theta(x), \quad c_{AB}(0, x) = 0$$

During the simulations, c_{A0} and c_{B0} were varied between 0.1 and 1000.0. The grid spacing was $\Delta x = 1.0$, and the numerical simulations were performed with the time step $\Delta\tau = 0.01$.

3. Results and Discussions

Figure 1 shows the spatial distribution of the precipitation patterns at two different initial concentration sets. In both cases, precipitation waves are observed. At the beginning of the simulation, the thickness of the band increases up to a certain value, and then, the width of the migration band (precipitation wave) is constant (in time) after some transient period. This

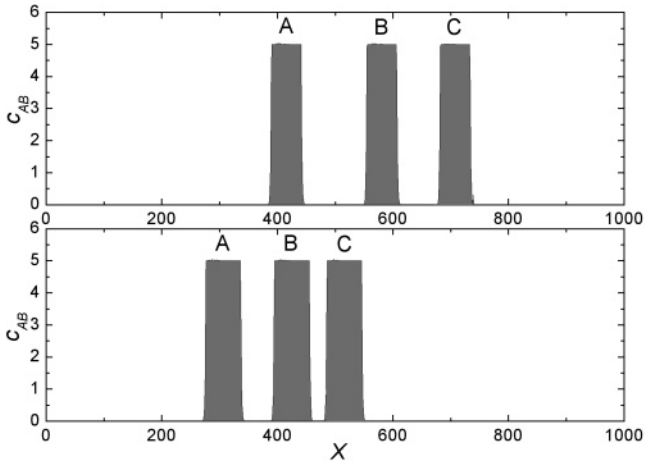

Figure 1. Spatial distribution of the precipitate for different initial concentration sets (c_{A0}, c_{B0}) of the outer and inner electrolytes at (A) $\tau = 7 \times 10^4$, (B) $\tau = 14 \times 10^4$, and (C) $\tau = 21 \times 10^4$: (top) $c_{A0} = 1000$, $c_{B0} = 200$; (bottom) $c_{A0} = 1000$, $c_{B0} = 400$.

basic observation is in good agreement with the experimental results. The evolution of a single band follows purely diffusive kinetics along the diffusion column, which is the direct consequence of the diffusion behavior of the outer electrolyte.

The effect of the initial concentration of the inner and outer electrolytes on the propagation of waves was also investigated. We introduce the center of gravity ($X_C(\tau)$) of the precipitation wave to describe the migrating band position as

$$X_C(\tau) = \frac{\sum_{i=1}^{N} c_{ABi}(\tau) X_i}{\sum_{i=1}^{N} c_{ABi}(\tau)}$$

where $c_{ABi}(\tau)$ is the amount of the precipitate in the ith grid point at τ, X_i is the position of the ith grid point measured from the junction point of the two electrolytes, and N is the number of grid points ($N = 2200$ in the present simulations).

In Figure 2, X_C is plotted versus $\tau^{1/2}$ for some initial concentration sets. The correlation between two variables is linear except for the first transient period. The propagation of the precipitation wave is slower for higher initial concentrations of the inner electrolyte (c_{B0}) at fixed c_{A0} (Figure 2a). In the reverse case (fixed c_{B0}), the trend is the opposite: increasing the initial concentration of the outer electrolyte (c_{A0}) results in a faster motion (Figure 2b). The propagation velocity in a square root time scale depends nonlinearly on c_{A0} and c_{B0}.

Variation of the initial concentrations of the electrolytes has a significant effect on the pattern structure. All parameters were the same, and only c_{A0} and c_{B0} were varied in the simulations. First, the thick band evolves, and then, this either remains a traveling heterogeneous wave or develops into discrete moving Liesegang bands. The possible moving patterns are shown in Figure 3. These are the precipitation wave (Figure 3a), the

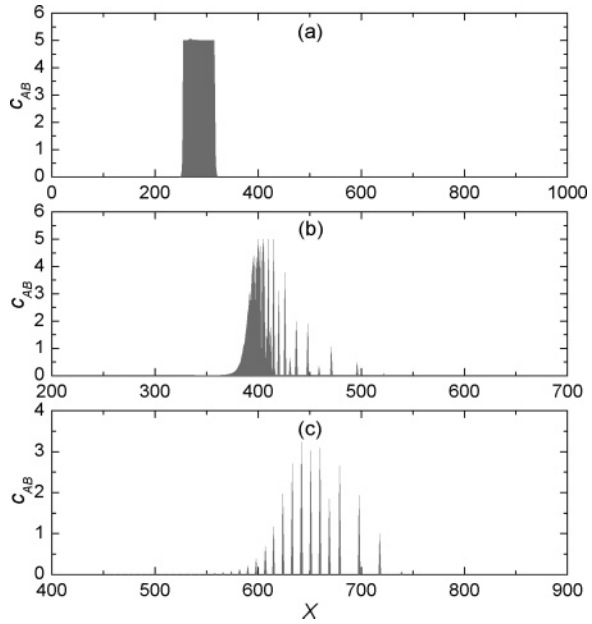

Figure 3. Structures of the moving precipitation patterns for different initial concentration sets of the outer and inner electrolytes at $\tau = 6 \times 10^4$: (a) $c_{A0} = 1000$, $c_{B0} = 400$; (b) $c_{A0} = 60$, $c_{B0} = 10$; (c) $c_{A0} = 60$, $c_{B0} = 2$.

moving Liesegang pattern (Figure 3c), and the mixed pattern (Figure 3b), where the former mentioned patterns coexist. A single wide precipitation band nearer to the junction point of the electrolytes can be observed; further, the band system develops. A detailed study was performed to investigate the dependence of the pattern structure on c_{A0} and c_{B0}, as is illustrated in Figure 4. In the case of extremely low initial concentrations of the electrolytes, there is no pattern formation, because the product of the local concentrations does not exceed the nucleation threshold. At higher c_{A0} and low c_{B0}, there was also no pattern formation observed, because all of the precipitate is redissolved due to the complex formation in high excess of the outer electrolyte. At relatively higher but still low c_{A0} and c_{B0}, moving Liesegang pattern formation was observed, while, at high concentrations for both species, the precipitation wave phenomenon is produced. For intermediate initial concentrations

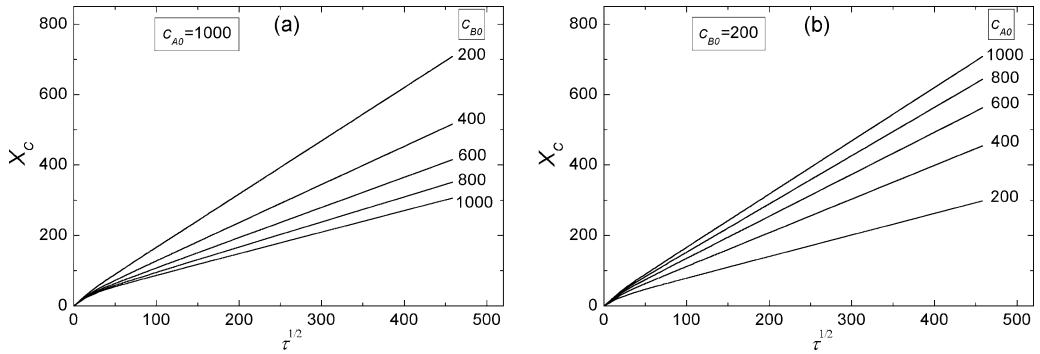

Figure 2. Evolution of precipitation waves for different initial concentration sets of the inner (a) and outer (b) electrolytes, respectively (the concentration of the outer (inner) electrolyte was held fixed).

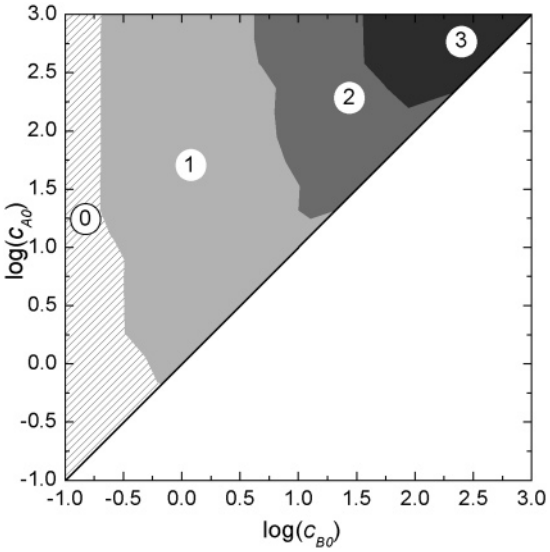

Figure 4. Existing patterns as a function of the initial concentration of the inner (c_{B0}) and outer (c_{A0}) electrolytes on a logarithmic scale at $\tau = 6 \times 10^4$. The pattern formation was classified as (0) no precipitation, (1) moving Liesegang bands, (2) precipitation wave + moving Liesegang bands, and (3) precipitation wave.

of the outer and inner electrolytes, the mixed patterns are developed and existed.

In summary, the crossover from the traveling wave to the moving Liesegang pattern is investigated and reproduced by numerical simulations. The phase portrait indicates the region (window) where these two structures coexist. This result can help find and design for the first time mixed patterns in experiments.

Acknowledgment. We are very grateful to Prof. Zoltán Rácz and Judit Zádor for helpful discussions. We acknowledge the support of the OTKA Postdoctoral Fellowship (OTKA D048673) and the OMFB grant 00585/2003 (IKTA5-137) of the Hungarian Ministry of Education.

References and Notes

(1) Liesegang, R. E. *Naturwiss. Wochenschr.* **1896**, *11*, 353.
(2) Marko, F.; Pivko, D.; Hurai, V. *Geol. Q.* **2003**, *47*, 241.
(3) Xie, D. T.; Wu, J. G.; Xu, G. X.; Qi, O. Y.; Soloway, R. D.; Hu, T. D. *J. Phys. Chem. B* **1999**, *103*, 8602.
(4) Chopard, B.; Luthi, P.; Droz, M. *Phys. Rev. Lett.* **1994**, *72*, 1384.
(5) Chopard, B.; Luthi, P.; Droz, M. *J. Stat. Phys.* **1994**, *76*, 661.
(6) Izsák, F.; Lagzi, I. *Chem. Phys. Lett.* **2003**, *371*, 321.
(7) Lagzi, I.; Izsák, F. *Phys. Chem. Chem. Phys.* **2003**, *5*, 4144.
(8) Dee, G. T. *Phys. Rev. Lett.* **1986**, *57*, 275.
(9) LeVan, M. E.; Ross, J. *J. Phys. Chem.* **1987**, *91*, 6300.
(10) Chernavskii, D. S.; Polezhaev, A. A.; Müller, S. C. *Physica D* **1991**, *54*, 160.
(11) Polezhaev, A. A.; Müller, S. C. *Chaos* **1994**, *4*, 631.
(12) Büki, A.; Kárpáti-Smidróczki, É.; Zrínyi, M. *J. Chem. Phys.* **1995**, *103*, 10387.
(13) Büki, A.; Kárpáti-Smidróczki, É.; Zrínyi, M. *Physica A* **1995**, *220*, 357.
(14) Krug, H.-J.; Brandtstädter, H. *J. Phys. Chem. A* **1999**, *103*, 7811.
(15) Chacron, M.; L'Heureux, I. *Phys. Lett. A* **1999**, *263*, 70.
(16) Antal, T.; Droz, M.; Magnin, J.; Pekalski, A.; Rácz, Z. *J. Chem. Phys.* **2001**, *114*, 3770.
(17) Izsák, F.; Lagzi, I. *J. Chem. Phys.* **2004**, *120*, 1837.
(18) Antal, T.; Droz, M.; Magnin, J.; Rácz, Z.; Zrínyi, M. *J. Chem. Phys.* **1998**, *109*, 9479.
(19) Droz, M.; Magnin, J.; Zrínyi, M. *J. Chem. Phys.* **1999**, *110*, 9618.
(20) Müller, S. C.; Ross, J. *J. Phys. Chem. A* **2003**, *107*, 7997.
(21) Ostwald, W. *Kolloid-Z.* **1925**, *36*, 380.
(22) Wagner, C. *J. Colloid Sci.* **1950**, *5*, 85.
(23) Prager, S. *J. Chem. Phys.* **1956**, *25*, 279.
(24) Keller, J. B.; Rubinow, S. I. *J. Chem. Phys.* **1981**, *74*, 5000.
(25) Feeney, R.; Schmidt, S. L.; Strickholm, P.; Chandam, J.; Ortoleva, P. *J. Chem. Phys.* **1983**, *78*, 1293.
(26) Venzl, G. *J. Chem. Phys.* **1986**, *85*, 1996.
(27) Venzl, G. *J. Chem. Phys.* **1986**, *85*, 2006.
(28) Rácz, Z. *Physica A* **1999**, *274*, 50.
(29) Sultan, R. F. *Phys. Chem. Chem. Phys.* **2002**, *4*, 1253.
(30) Zrínyi, M.; Gálfi, L.; Smidróczki, É.; Rácz, Z.; Horkay, F. *J. Phys. Chem.* **1991**, *95*, 1618.
(31) Sultan, R.; Halabieh, R. *Chem. Phys. Lett.* **2000**, *332*, 331.
(32) Hilal, N.; Sultan, R. *Chem. Phys. Lett.* **2003**, *374*, 183.
(33) Das, I.; Pushkarna, A.; Agrawal, N. R. *J. Phys. Chem.* **1989**, *93*, 7269.
(34) Sultan, R.; Sadek, S. *J. Phys. Chem.* **1996**, *100*, 16912.
(35) Nasreddine, V.; Sultan, R. *J. Phys. Chem. A* **1999**, *103*, 2934.
(36) Al-Ghoul, M.; Sultan, R. *J. Phys. Chem. A* **2001**, *105*, 8053.
(37) Lagzi, I. *J. Phys. Chem. B* **2003**, *107*, 13750.